




## Multistage quantum swapping of vacuum-one-photon entanglement

Lu-Feng Qiao <sup>1</sup>, Zhi-Qiang Jiao,<sup>1</sup> Xiao-Yun Xu,<sup>1</sup> Jun Gao,<sup>1</sup> Zhe-Yong Zhang <sup>1</sup>, Ruo-Jing Ren,<sup>1</sup> Wen-Hao Zhou,<sup>1</sup>  
Xiao-Wei Wang,<sup>1</sup> and Xian-Min Jin <sup>1,2,3,\*</sup>

<sup>1</sup>*Center for Integrated Quantum Information Technologies (IQIT), School of Physics and Astronomy and State Key Laboratory of Advanced Optical Communication Systems and Networks, Shanghai Jiao Tong University, Shanghai 200240, China*

<sup>2</sup>*CAS Center for Excellence and Synergetic Innovation Center in Quantum Information and Quantum Physics, University of Science and Technology of China, Hefei, Anhui 230026, China*

<sup>3</sup>*TuringQ Co., Ltd., Shanghai 200240, China*



(Received 3 October 2020; accepted 26 May 2021; published 17 August 2021)

Vacuum-one-photon entanglement can serve as an alternative to many protocols implemented by two-photon states, and also exhibits its own practical advantages. Quantum swapping plays a central role in both constructing photonic quantum computers and quantum networks. However, the phase-sensitivity in free space makes it very challenging to scale quantum swapping of vacuum-one-photon entanglement up to multistage, especially to large-scale quantum networks. Here, we implement multistage quantum swapping of vacuum-one-photon entanglement on a three-dimensional reconfigurable photonic chip. We also propose and experimentally demonstrate a prototype of a fully connected multipartite network based on multistage quantum swapping. Our results provide an integrated, scalable, and portable solution of multistage quantum swapping, showing the potential as a crucial element of the all-photonic quantum information processing.

DOI: [10.1103/PhysRevA.104.022415](https://doi.org/10.1103/PhysRevA.104.022415)

### I. INTRODUCTION

Entanglement is a unique and the most essential resource in quantum physics, and lives at the heart of many counterintuitive tasks, like quantum teleportation [1–4], quantum Fourier transformation [5], and quantum-enhanced security [6–8]. These tasks are the kernels of modern quantum technologies, like quantum communication [9–11], quantum machine learning [12], constructing quantum networks [13], and building universal quantum computers [14,15]. In all these application scenarios, entanglement can live in a variety of different carriers and degrees of freedom, among which, the vacuum-one-photon entanglement [Eq. (1)] may be the most exotic one. Its orthogonal basis in Hilbert space is the single-photon state and the vacuum state [16], which can be expressed as

$$|\psi\rangle = |0\rangle_A |1\rangle_B + e^{i\phi} |1\rangle_A |0\rangle_B, \quad (1)$$

where  $|0\rangle_A |1\rangle_B$  denotes vacuum in mode  $A$  and one photon in mode  $B$ , and vice versa.

The bizarre feature of vacuum-one-photon entanglement attracts many fundamental interests including the mere existence [17], the nonlocality [18], and Einstein-Podolsky-Rosen steering [19]. Vacuum-one-photon entanglement is much different from all the other types of entanglement since there is only one photon included in this bipartite state, but the entanglement can be also up to 1 ebit if we choose mode representation other than particle representation [20]. The information carrier (widely known as qubit) in the vacuum-one-photon entanglement is the electromagnetic field mode

[18]. Nowadays, vacuum-one-photon entanglement is widely exploited in many aspects ranging from quantum repeater [21], teleportation [16,22], entanglement swapping [23,24], purification [25], multipartite entanglement [26,27], to heralded photon amplification [28]. The vacuum-one-photon entanglement possesses a few distinct advantages. First, the entanglement is easy to generate, and one of the simplest ways is to send a single photon through a balanced beam splitter (BS). Secondly, such entanglement can be swapped and purified simply by linear optics. As it transfers less photon than the two-photon entanglement that will gain the square-root dependence of the key rate on the channel transmittance [29]. And it requires fewer resources than other protocol when it is used to implement the quantum repeater, so it is less sensitive to quantum memory and the efficiency of the photon detectors [21]. Last but not least, the combination of temporal multiplexing and vacuum-one-particle entanglement can reach high entanglement distribution rates for an efficient quantum repeater [30].

However, the phase sensitivity of the vacuum-one-particle entanglement remains a challenge in building large-scale quantum networks. Here, we surmount this challenge by implementing quantum swapping of the vacuum-one-photon entanglement on a photonic chip. After the demonstration of the quantum gate in the integrated photonic chip in 2008 [31], many crucial works have gradually acknowledged integrated photonics platforms because of their ability for large-scale information processing [32]. There are several typical platforms, which possess different advantages [33–36]. In this work, we use the femtosecond laser direct writing technique, which has the three-dimensional (3D) fabrication ability that is different from other platforms [37]. By using a 3D structure, the photonic circuit will be much more simplified.

\*xianmin.jin@sjtu.edu.cn

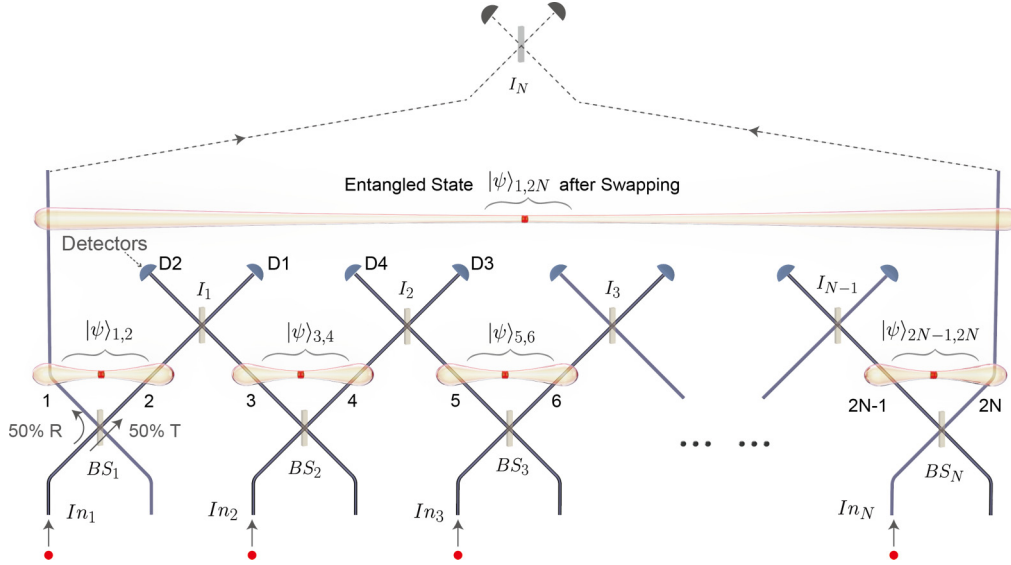


FIG. 1. Schematic of multistage quantum swapping of vacuum-one-photon entanglement. The 50:50 BS<sub>*i*</sub>, (*i* = 1, 2, 3, *N*) are used to generate the vacuum-one-photon entanglements. When two photons are injected into *In*<sub>1</sub> and *In*<sub>2</sub>, respectively and simultaneously, the interference will occur at a 50:50 BS denoted as *I*<sub>1</sub>. Then the entanglement will be swapped to paths 1 and 4. The protocol can be further scaled to *N* photons. When the single photons are injected *N* input ports simultaneously, the electromagnetic field mode of photon 1 in path 1 and the electromagnetic field mode in photon *N* in path 2*N* will be entangled after a series of single-photon interferences in BSs (*I*<sub>1</sub>, *I*<sub>2</sub>, *I*<sub>3</sub>, and etc.). An additional BS *I*<sub>*N*</sub> can be used to verify the entangled state  $|\psi\rangle_{1,2N}$ .

We employ the femtosecond laser direct writing technique to prepare a 3D photonic circuit for implementation and verification on a single chip, and prepare the on-chip phase controller to have a reconfigurable fashion. We further extend the protocol to multistage entanglement swapping [38] for vacuum-one-photon entanglement. Moreover, we propose a prototype of a fully connected multipartite network, which is inherently scalable and its achievable scale is only limited by the brightness of the single-photon source.

## II. PROTOCOL

In Fig. 1, we show the diagram of the quantum swapping of vacuum-one-photon entanglement. When a photon enters a 50:50 beam splitter (BS), it has an equal chance either transmitting (T) the BS or being reflected (R) by the BS. The generated state is a vacuum single-photon entangled state:  $|\psi\rangle = \frac{1}{\sqrt{2}}(|1\rangle_T|0\rangle_R + i|0\rangle_T|1\rangle_R)$ , where the phase term  $\frac{\pi}{2}$  comes from the difference in these two paths.

The entanglement is in the electromagnetic field's mode of a photon. As shown in Fig. 1, three 50:50 BS can be assembled into the elementary case of the protocol. The two photons are injected into *In*<sub>1</sub> and *In*<sub>2</sub>, respectively and simultaneously. The first two BSs (BS<sub>1</sub> and BS<sub>2</sub>) are used to generate the entanglement. Considering the phase difference in paths 1, 2, 3, and 4, the generated entangled state can be expressed as  $|\psi\rangle_{1,2} = \frac{1}{\sqrt{2}}(|0\rangle_1|1\rangle_2 + e^{i\theta^{(1)}}|1\rangle_1|0\rangle_2)$ , and  $|\psi\rangle_{3,4} = \frac{1}{\sqrt{2}}(|0\rangle_3|1\rangle_4 + e^{i\theta^{(2)}}|1\rangle_3|0\rangle_4)$ . The BS *I*<sub>1</sub> is used as the single-photon interference part, where the total state can be

expressed as

$$\begin{aligned} & |\psi\rangle_{1,2} \otimes |\psi\rangle_{3,4} \\ &= \frac{1}{2} \left[ \frac{1}{\sqrt{2}}(|0\rangle_1|1\rangle_4 + e^{i(\theta^{(1)}+\theta^{(2)})}|1\rangle_1|0\rangle_4)|\phi^1\rangle \right. \\ & \quad \left. - \frac{1}{\sqrt{2}}(|0\rangle_1|1\rangle_4 - e^{i(\theta^{(1)}+\theta^{(2)})}|1\rangle_1|0\rangle_4)|\phi^2\rangle \right] \\ & \quad + \frac{1}{2} e^{i\theta^{(1)}}|1\rangle_1|1\rangle_4|\phi^3\rangle + \frac{1}{2} e^{i\theta^{(2)}}|0\rangle_1|0\rangle_4|\phi^4\rangle, \quad (2) \end{aligned}$$

where  $|\phi^1\rangle = \frac{1}{\sqrt{2}}(|0\rangle_2|1\rangle_3 + |1\rangle_2|0\rangle_3) = |1\rangle_{D1}|0\rangle_{D2}$ ,  $|\phi^2\rangle = \frac{1}{\sqrt{2}}(|0\rangle_2|1\rangle_3 - |1\rangle_2|0\rangle_3) = |0\rangle_{D1}|1\rangle_{D2}$ ,  $|\phi^3\rangle = |0\rangle_2|0\rangle_3 = |0\rangle_{D1}|0\rangle_{D2}$ , and  $|\phi^4\rangle = |1\rangle_2|1\rangle_3 = \frac{1}{\sqrt{2}}(|0\rangle_{D1}|2\rangle_{D2} - |2\rangle_{D1}|0\rangle_{D2})$ .

We can decompose the total state with different cases in *I*<sub>1</sub>.  $|\phi^1\rangle$  implies a single photon arrives at detector D1 while no photon arrives at detector D2 after *I*<sub>1</sub>. So the detector D1 will herald the entangled state  $\frac{1}{\sqrt{2}}(|0\rangle_1|1\rangle_4 + e^{i(\theta^{(1)}+\theta^{(2)})}|1\rangle_1|0\rangle_4)$ . Similarly, the detector D2 will herald the entangled state  $\frac{1}{\sqrt{2}}(|0\rangle_1|1\rangle_4 - e^{i(\theta^{(1)}+\theta^{(2)})}|1\rangle_1|0\rangle_4)$ . In both cases, the entanglement in 1 and 2, and entanglement in 3 and 4 are swapped to 1 and 4. A phase shifter can be added in path 1 to change the relative phase between paths 1 and 4. When the state after *I*<sub>1</sub> is  $|\phi^3\rangle$  or  $|\phi^4\rangle$ , the swapping fails. The probability of success is 50%, as the no-go theory [39] says; the complete Bell-state measurement cannot be achieved and exceed 50% to distinguish the state without nonlinear effect [40], hyperentanglement [41], a large number of auxiliary qubits [42], or other more sophisticated technology. The success probability decreases exponentially with the number of stages, which

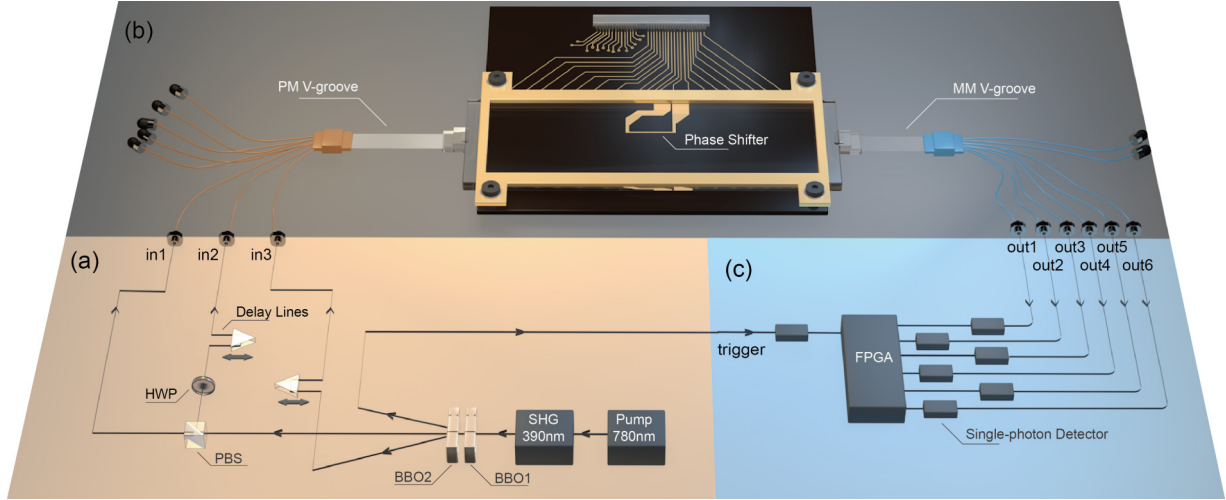


FIG. 2. Experimental setup. (a) The photon source. Four channels of single photons are prepared via SPDC. A 390-nm laser pulse pumps two BBO crystals in a cascaded configuration. BBO1 produces a pair of 780-nm photons, whose propagation direction overlaps with the pump light, while the photon pairs produced by BBO2 have a  $3^\circ$  angle offset. The first pair of photons have different polarizations (H and V) which can be separated by a PBS. Three channels are injected into the photonic chip after proper polarization control, and the fourth one is employed as the trigger signal. Two external delay lines are used to synchronize the four photons. (b) The integrated photonic chip. Two V-groove fiber arrays [the polarization-maintaining (PM) V groove at the input end and the multimode (MM) V groove at the output] are coupled to both facets of the photonic chip. An active gold-coated phase controller is printed on the surface of the chip. (c) The detection module. All the output photons are registered by single-photon detectors. The corresponding electronic signals are recorded and analyzed by a homemade FPGA to get the coincidence data.

can be improved by the advances in the photon source or measurement technology.

The vacuum-one-photon entanglement swapping can easily be expanded to multistages. After the first process, the entanglement state is in 1 and 4, for example,  $|\psi\rangle_{1,4} = \frac{1}{\sqrt{2}}(|0\rangle_1|1\rangle_4 + e^{i(\theta^{(1)}+\theta^{(2)})}|1\rangle_1|0\rangle_4)$ . If another photon is injected to In<sub>3</sub>, the entangled state  $|\psi\rangle_{5,6} = \frac{1}{\sqrt{2}}(|0\rangle_5|1\rangle_6 + e^{i\theta^{(3)}}|1\rangle_5|0\rangle_6)$  is produced. And

$$\begin{aligned} |\psi\rangle_{1,4} \otimes |\psi\rangle_{5,6} &= \frac{1}{2} \left[ \frac{1}{\sqrt{2}}(|0\rangle_1|1\rangle_6 + e^{i(\theta^{(1)}+\theta^{(2)}+\theta^{(3)})}|1\rangle_1|0\rangle_6)|\phi^1\rangle \right. \\ &\quad \left. - \frac{1}{\sqrt{2}}(|0\rangle_1|1\rangle_6 - e^{i(\theta^{(1)}+\theta^{(2)}+\theta^{(3)})}|1\rangle_1|0\rangle_6)|\phi^2\rangle \right] \\ &\quad + \frac{1}{2} e^{i(\theta^{(1)}+\theta^{(2)})}|1\rangle_1|1\rangle_6|\phi^3\rangle + \frac{1}{2} e^{i\theta^{(3)}}|0\rangle_1|0\rangle_6|\phi^4\rangle, \quad (3) \end{aligned}$$

where  $|\phi^1\rangle = \frac{1}{\sqrt{2}}(|0\rangle_4|1\rangle_5 + |1\rangle_4|0\rangle_5) = |1\rangle_{D3}|0\rangle_{D4}$ ,  $|\phi^2\rangle = \frac{1}{\sqrt{2}}(|0\rangle_4|1\rangle_5 - |1\rangle_4|0\rangle_5) = |0\rangle_{D3}|1\rangle_{D4}$ ,  $|\phi^3\rangle = |0\rangle_4|0\rangle_5 = |0\rangle_{D3}|0\rangle_{D4}$ , and  $|\phi^4\rangle = |1\rangle_4|1\rangle_5 = \frac{1}{\sqrt{2}}(|0\rangle_{D3}|2\rangle_{D4} - |2\rangle_{D3}|0\rangle_{D4})$ .

$|\phi^1\rangle$  is a Bell-like state, and it implies the single photon arrives at detector D3 and does not arrive at detector D4. And as stated above,  $|\psi\rangle_{1,4} = \frac{1}{\sqrt{2}}(|0\rangle_1|1\rangle_4 + e^{i(\theta^{(1)}+\theta^{(2)})}|1\rangle_1|0\rangle_4)$  is heralded by the detector D1. So D1&D3 (the detector D1 and the detector D3 together) will herald the entangled state  $\frac{1}{\sqrt{2}}(|0\rangle_1|1\rangle_6 + e^{i(\theta^{(1)}+\theta^{(2)}+\theta^{(3)})}|1\rangle_1|0\rangle_6)$ . Similarly, D1&D4 (the detector D1 and the detector D4 together) will herald the entangled state  $\frac{1}{\sqrt{2}}(|0\rangle_1|1\rangle_6 - e^{i(\theta^{(1)}+\theta^{(2)}+\theta^{(3)})}|1\rangle_1|0\rangle_6)$ . It can be easily deduced that D2&D4 will herald the same entangled

state as D1&D3, while D2&D3 will herald the same entangled state as D1&D4.

After two interferometers  $I_1$  and  $I_2$ , the entanglement can be swapped to paths 1 and 6. As shown in Fig. 1, photon 1's electromagnetic field mode in path 1 and photon  $N$ 's electromagnetic field mode in path  $2N$  will be entangled after a series of single-photon interferences. An additional BS  $I_N$  can be used to verify the entangled state  $|\psi\rangle_{1,2N}$ . The scheme is simple but elegant since only one phase shifter is needed. We theoretically derive that all phase differences in  $2N$  paths can be reduced into one path. The crosstalk between different phase shifters in the photonic chip often hinders the programmability and scalability, thus our protocol provides an alternative solution by merging all the phase differences into one path.

### III. EXPERIMENTS

The experimental setup is made up of three modules: the single-photon sources, the integrated photonic chip, and the detection module. Two pairs of single photons are generated by spontaneous parametric downconversion (SPDC) and synchronized by delay lines; see Fig. 2(a). The first BBO crystal is co-linear phase matching while the second one is type-II phase matching in the beamlike scheme [43]. The generated photons are all shaped by 3-nm bandpass filters and then collected into single-mode polarization-maintaining fibers. The photons can be coupled into the integrated photonic chip directly from free space for the one-stage entanglement swapping experiment. For the multistage experiment, we let the chip butt-coupled to two V-groove fiber arrays at two end facets, which makes the whole device more portable and convenient, as illustrated in Fig. 2(b). The phase shifter is directly fabricated from a gold

TABLE I. 50:50 coupling lengths at different depths.

Sample	I	II	III	IV
Depth ( $\mu\text{m}$ )	25	50	75	100
Coupling length (mm)	0.75	1.05	1.10	1.20

film coated on the surface of the chip substrate by using the femtosecond laser-induced forward transfer technique [44]. The fabrication process of the phase shifter is as follows. We first use the ultrasonic wave to clean the chip surface. Then the chip is coated with 99.99% purity gold by evaporation coating. Part of the gold is removed to form a resistor pattern using laser ablation. The working part is a very slim gold layer, making it have a value of several tens  $\Omega$  for the resistor. The phase shifter has two pins, which are directly connected to a power supply, and works as a heater. The heater can adjust the phase of photons in the waveguide buried under the surface. The response time is about several tens of milliseconds.

After the operations defined by the photonic chip, all the photons out of the chip are measured together with the trigger signals. An array of avalanche photodiodes (APDs) register all the modes to obtain the corresponding output signals [Fig. 2(c)], and the coincidence counts are recorded and given by a homemade field-programmable gate array (FPGA).

The quality of 50:50 BS is at the core of the vacuum-one-photon entanglement swapping. Such device is involved in entanglement preparation, single-photon interference, and verification process. The phase shifter is implanted on one arm of the entangled state, enabling us to observe the non-classical oscillation curves. All the desired components can be integrated into a single photonic chip due to the compact and flexible fabrication capability guaranteed by the femtosecond laser direct writing technique [37,45–47]. The balanced BS is achieved by evanescent coupling; the curvature of the BS arm is specially chosen to reach low loss [48]. Several coupling widths have been first tested and 10  $\mu\text{m}$  is selected for quick coupling while keeping the profiles of the two modes from overlapping. Then the coupling lengths are scanned to achieve the 50:50 splitting ratio, where single photons have equal probability entering each arm of the BS, thus generating a maximally entangled state.

The 3D capability of the femtosecond laser direct writing technique allows us to fully take advantage of different depths, beyond the limitation of single-layer circuits. As shown in Fig. 1, single-photon interference on both  $I_1$  and  $I_N$  is challenging when only using planar layout, but comparably straightforward using 3D structures. In our experiment, we fabricate  $I_i$  ( $i = 1, 2, 3, \dots, N - 1$ ) and  $I_N$  under different depths, and all the output waveguides are transformed to the same depth with equal spacing of 127  $\mu\text{m}$ . In our experiment, parameters under at least two different depths for the BS are needed. As shown in Table I, the coupling coefficients at different depths of the chip are different. When the BS is closer to the upper surface, the corresponding coupling coefficient is larger. We therefore can achieve balanced BS operation by tuning the coupling length according to the characterized coefficient.

As shown in Fig. 3(a), two correlated photons generated in the same BBO crystal are first injected into the entanglement

generation part of the chip; the coincidence rates of the source are about 100 kHz. The photons are both prepared in horizontal polarization, the Hong-Ou-Mandel (HOM) visibility of the source is tested in a fiber BS, which gives a value of 93%. We have also performed the two-photon interference tests on the BSs of the single-photon interference part and verification part; the HOM-dips obtained at these two BSs are shown in Fig. 3(b). The corresponding visibilities are 82.7% and 75.4%, respectively.

The phenomenon of entanglement swapping can be observed in the range where HOM-dip occurs. These interference curves reveal the nonclassical trait. We alter the driving voltage on the phase shifter and monitor the twofold coincidence rates of each output. The results are shown in Fig. 3(c); the coincidence rates of D1&D3 (D1&D2) vary together with D2&D4 (D3&D4). We numerically fit the curve of D1&D3 with a sine function, and the D1&D2 curve automatically fits a sine function with the same frequency and a phase difference of  $\pi$ . To be more specific, the peak in the D1&D3 curve indicates that we have successfully performed the quantum swapping, and the resulting entanglement can be well analyzed by varying the phases, showing oscillated curve at each output. We have also tested the case out of the range of HOM interference; all the coincidence rates remain invariant when changing the phase.

The vacuum-one-photon entanglement swapping protocol can be further extended to multistage quantum swapping. As shown in Fig. 4(a), the chip adds two input and output ports, respectively. Four single photons are generated by two SPDC sources. We choose one of the four photons as the trigger signal and inject the other three photons into the photonic chip via a V-groove fiber array. The post-selection on fourfold coincidence rates of different outputs identifies an effective two-stage entanglement swapping and provides the information of resulting states; see Figs. 4(b)–4(e). The fidelities can be calculated as [16]

$$F = \langle \psi_{\text{in}} | \psi_{\text{out}} \rangle = (1 + V)/2. \quad (4)$$

The average fidelity in our experiment is  $82.8 \pm 3.5\%$ , which well exceeds the classical limit (66.7%) with four standard deviations. Our work presents a post-selection multistage entanglement swapping but the scheme can be prompted for other demonstrations by including more sophisticated techniques, like photon-number-resolving detectors.

#### IV. DISCUSSION

Our multistage quantum swapping can also function as an integrated server for a star-topology quantum network where quantum states can be swapped between arbitrary modes. For example, as shown in Figs. 4(b) and 4(c), the fourfold coincidence counts of D1&D3&D5&D7 and D2&D3&D5&D7 are fitted by sinusoidal functions with a  $\pi$  phase flip. Such a process can entangle mode  $b$  and mode  $c$ , which do not interact with each other [see Fig. 4(f)]. This is a typical multistage entanglement swapping process. Here,  $I_1$  is used to verify the entangled state after swapping.

In our scheme, the kernels of teleportation and entanglement swapping share the same spirit. Take Fig. 4(h) as an example; here  $I_3$  is used as the verification part, while  $I_1$

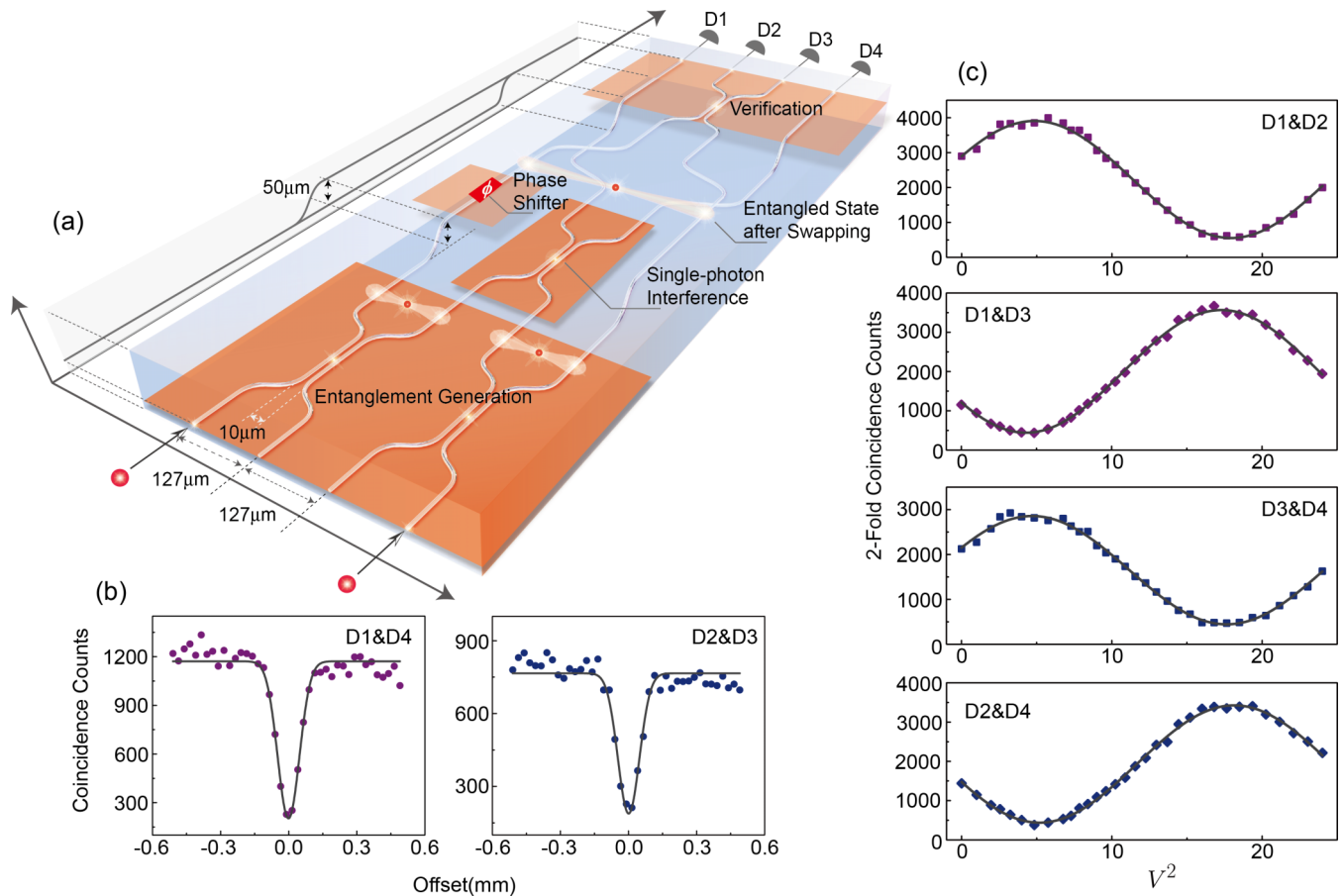


FIG. 3. The element case of vacuum-one entanglement swapping and the structure of photonic chip. (a) Schematic of the chip design. The chip is made up of the entanglement generation, interference, phase shifter, and verification. By taking full advantage of 3D fabrication capability, the interference and verification parts are inscribed under different depths. (b) HOM-dips on the BSs used for the interference (D1&D4) and the verification (D2&D3). (c) Experimental results. The coincidence results of D1&D3, D1&D2, D3&D4, and D2&D4 form oscillation curves when tuning the voltage ( $V$ ) applied to the phase shifter.

and  $I_2$  are used as the single-photon interference parts. In this case, the server realizes quantum teleportation between mode  $a$  and mode  $f$ . Similarly, if we choose  $I_2$  and  $I_3$  as the single-photon interference parts, mode  $b$  and mode  $c$  can be entangled through the entanglement swapping. For the diagonal direction swapping between mode  $a$  and mode  $d$ , this can be realized by directly interfering mode  $b$  and mode  $c$ . In this way, our platform can function as a fully connected network and further be expanded to a larger  $n$ -client network, enabling multiparty communication and quantum blockchain [49]. The quantum network is also useful in quantum computation tasks [15], where the integration implementation is both suitable and stable.

For the quantum network in the long-distance quantum communications, the chips can work as a terminal equipment to realize the interference, and the long-distance transmission can be a hybrid system that uses optical fibers or free space. The phase stability of delivering quantum modes between stations is studied recently [50], which is technically solvable. The vacuum and single-photon superposition has also been proved to be a good medium by protocols like TF-QKD [51]. The protocol gains the square root dependence of the key rate on the channel transmittance and requires fewer resources

than other protocols. The on-chip single-photon source [52] may further reduce the loss of the interface loss.

We know TF-QKD is more efficient than other QKD protocols against channel loss [51]. It would be great if the protocols of multistage entanglement swapping can be applied into TF-QKD. These two protocols share the same features in encoding, sharing, and verifying qubits in the state space of vacuum and single photon. The enhanced TF-QKD is possible if we apply an active version multistage entanglement swapping associated with encoding on two remote terminals. The remote terminals can be analyzed by the local resonant field instead of interfering with each other directly.

In summary, we have experimentally demonstrated multistage quantum swapping of vacuum-one-photon entanglement. The entanglement generation, interference, and verification parts are all integrated into a single photonic chip with high stability and scalability. The on-chip active tuning allows us to analyze the resulting quantum states. The brightness of the photon source, the scalability of the photonic chip, and reconfigurable 3D circuit can be further improved. Our work demonstrates multistage quantum swapping with the capability of fully integrating state manipulation, phase control, and state verification into a single photonic chip, representing

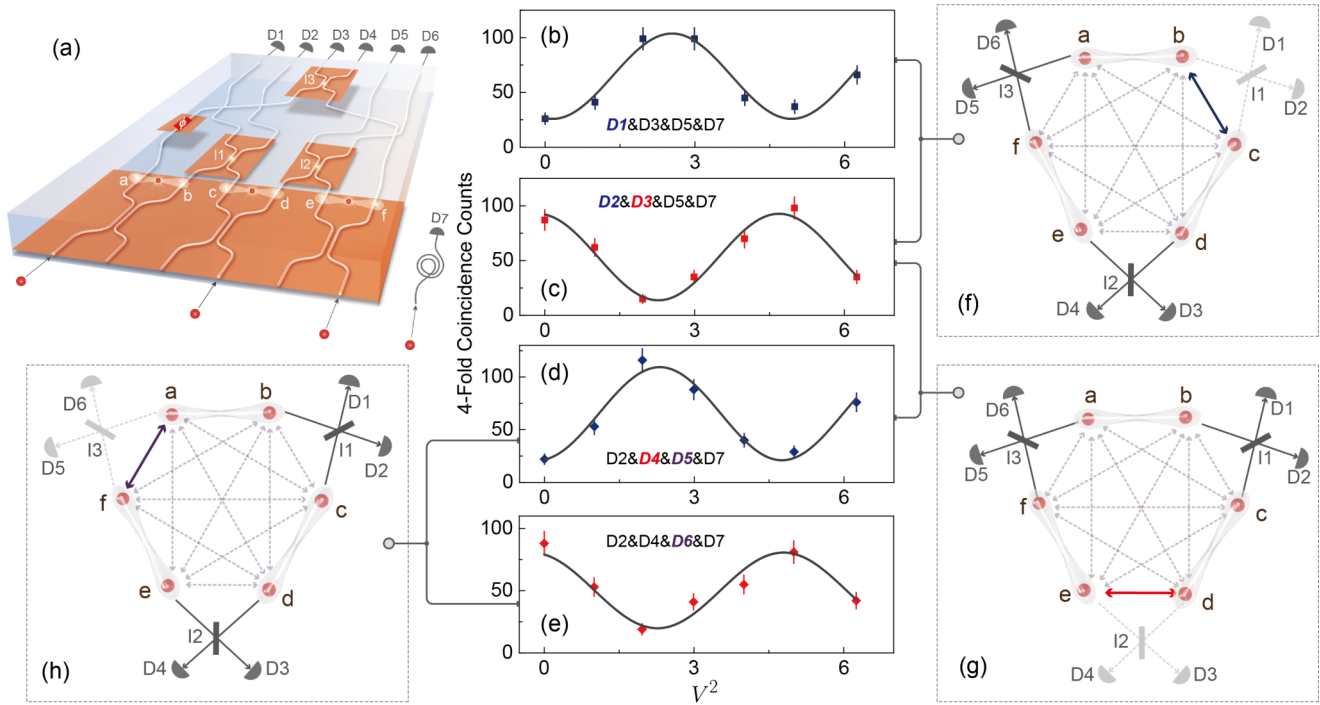


FIG. 4. Experimental results of multistage swapping. (a) The photonic chip is prompted to support three vacuum-one-photon entanglement states. (b)–(e) The experimental results of fourfold coincidence counts with three photons interfering in the photonic chip while the last one serving as the trigger. (f)–(h) Three cases of multistage entanglement swapping. (f) In this case, interferometer  $I_2$  and  $I_3$  work as the single-photon interference part. After the interference, mode  $b$  and mode  $c$  will be entangled, which did not interact with each other directly. This is a typical multistage entanglement swapping process.  $I_1$  is used to verify the entangled state after swapping. Similarly, in (g) mode  $e$  and mode  $d$  will be entangled while in (h) mode  $a$  and mode  $f$  will be entangled after the swapping process.

a substantial step forward to large-scale, all-photonic, all-on-chip quantum information processing.

ACKNOWLEDGMENTS

This research is supported by the National Key R&D Program of China (Grants No. 2019YFA0706302, No. 2019YFA0308700, and No. 2017YFA0303700); National Natural Science Foundation of China (NSFC) (Grants

No. 11904229, No. 61734005, No. 11761141014, and No. 11690033); Science and Technology Commission of Shanghai Municipality (STCSM) (Grants No. 20JC1416300 and No. 2019SHZDZX01); Shanghai Municipal Education Commission (SMEC) (Grant No. 2017-01-07-00-02-E00049); China Postdoctoral Science Foundation (Grant No. 2020M671091). X.-M.J. acknowledges additional support from a Shanghai talent program and support from Zhiyuan Innovative Research Center of Shanghai Jiao Tong University.

[1] D. Llewellyn *et al.*, Chip-to-chip quantum teleportation and multi-photon entanglement in silicon, *Nat. Phys.* **16**, 148 (2020).  
 [2] B. J. Metcalf *et al.*, Quantum teleportation on a photonic chip, *Nat. Photon.* **8**, 770 (2014).  
 [3] X.-M. Jin *et al.*, Experimental free-space quantum teleportation, *Nat. Photon.* **4**, 376 (2010).  
 [4] C. H. Bennett, G. Brassard, and C. Crépeau, Teleporting an Unknown Quantum State via Dual Classical and Einstein-Podolsky-Rosen Channels, *Phys. Rev. Lett.* **70**, 1895 (1993).  
 [5] L. Hales and S. Hallgren, An improved quantum Fourier transform algorithm and applications, in *Proceedings 41st Annual Symposium on Foundations of Computer Science* (IEEE, Piscataway, 2000), pp. 515-525.  
 [6] C. H. Bennett, and G. Brassard, Quantum cryptography: Public key distribution and coin tossing, in *Proceedings of IEEE International Conference on Computers, Systems and Signal Processing*, Vol. 175 (IEEE, New York, 1984), p. 8.  
 [7] V. Scarani, H. Bechmann-Pasquinucci, N. J. Cerf, M. Dušek, N. Lutkenhaus, and M. Peev, The security of practical quantum key distribution, *Rev. Mod. Phys.* **81**, 1301 (2009).  
 [8] P. W. Shor and J. Preskill, Simple Proof of Security of the BB84 Quantum Key Distribution Protocol, *Phys. Rev. Lett.* **85**, 441 (2000).  
 [9] N. Gisin and R. Thew, Quantum communication, *Nat. Photon.* **1**, 165 (2007).  
 [10] L.-M. Duan, M. D. Lukin, J. I. Cirac, and P. Zoller, Long-distance quantum communication with atomic ensembles and linear optics, *Nature (London)* **414**, 413 (2001).  
 [11] J.-W. Pan, C. Simon, C. Brukner, and A. Zeilinger, Entanglement purification for quantum communication, *Nature (London)* **410**, 1067 (2001).

- [12] J. Biamonte *et al.*, Quantum machine learning, *Nature (London)* **549**, 195 (2017).
- [13] J. I. Cirac, H. J. Zoller, and H. Mabuchi, Quantum State Transfer and Entanglement Distribution Among Distant Nodes in a Quantum Network, *Phys. Rev. Lett.* **78**, 3221 (1997).
- [14] J. L. O'Brien, Optical Quantum Computing, *Science* **318**, 1567 (2007).
- [15] E. Knill, R. Laflamme, and G. J. Milburn, A Scheme for Efficient Quantum Computation with Linear Optics, *Nature (London)* **409**, 46 (2001).
- [16] E. Lombardi, F. Sciarrino, S. Popescu, and F. De Martini, Teleportation of a Vacuum-One-Photon Qubit, *Phys. Rev. Lett.* **88**, 070402 (2002).
- [17] S. J. van Enk, Single-particle entanglement, *Phys. Rev. A* **72**, 064306 (2005).
- [18] S. M. Tan, D. F. Walls, and M. J. Collett, Nonlocality of a Single Photon, *Phys. Rev. Lett.* **66**, 252 (1991).
- [19] T. Guerreiro, F. Monteiro, A. Martin, J. B. Brask, T. Vértesi, B. Kozh, M. Caloz, F. Bussières, V. B. Verma, A. E. Lita *et al.*, Demonstration of Einstein-Podolsky-Rosen Steering Using Single-Photon Path Entanglement and Displacement-Based Detection, *Phys. Rev. Lett.* **117**, 070404 (2016).
- [20] H. M. Wiseman and John A. Vaccaro, Entanglement of Indistinguishable Particles Shared between Two Parties, *Phys. Rev. Lett.* **91**, 097902 (2003).
- [21] N. Sangouard, C. Simon, H. De Riedmatten, and N. Gisin, Quantum repeaters based on atomic ensembles and linear optics, *Rev. Mod. Phys.* **83**, 33 (2011).
- [22] M. Fuwa, S. Toba, S. Takeda, P. Marek, L. Mista, R. Filip, P. vanLoock, J. I. Yoshikawa, and A. Furusawa, Noiseless Conditional Teleportation of a Single Photon, *Phys. Rev. Lett.* **113**, 223602 (2014).
- [23] C. I. Osorio, Heralded photon amplification for quantum communication, *Phys. Rev. A* **86**, 023815 (2012).
- [24] F. Sciarrino, E. Lombardi, G. Milani, and F. De Martini, Delayed-choice entanglement swapping with vacuum-one-photon quantum states, *Phys. Rev. A* **66**, 024309 (2002).
- [25] D. Salart, Purification of Single-Photon Entanglement, *Phys. Rev. Lett.* **104**, 180504 (2010).
- [26] S. B. Papp, Characterization of Multipartite Entanglement for One Photon Shared Among Four Optical Modes, *Science* **324**, 764 (2009).
- [27] M. Gräfe, On-chip generation of high-order single-photon W-states, *Nat. Photon.* **8**, 791 (2014).
- [28] S. Kocsis, G. Y. Xiang, T. C. Ralph, and G. J. Pryde, Heralded noiseless amplification of a photon polarization qubit, *Nat. Phys.* **9**, 23 (2013).
- [29] M. Lucamarini *et al.*, Overcoming the rate-distance limit of quantum key distribution without quantum repeaters, *Nature (London)* **557**, 400 (2018).
- [30] C. Simon, H. deRiedmatten, M. Afzelius, N. Sangouard, H. Zbinden, and N. Gisin, Quantum Repeater with Photon Pair Sources and Multimode Memories, *Phys. Rev. Lett.* **98**, 190503 (2007).
- [31] A. Politi *et al.*, Silica-on-silicon waveguide quantum circuits, *Science* **320**, 646 (2008).
- [32] J. Wang *et al.*, Integrated photonic quantum technologies, *Nat. Photon.* **14**, 273 (2020).
- [33] P. Shadbolt *et al.*, Generating, manipulating and measuring entanglement and mixture with a reconfigurable photonic circuit, *Nat. Photon.* **6**, 45 (2012).
- [34] L. Sansoni, F. Sciarrino, G. Vallone, P. Mataloni, A. Crespi, R. Ramponi, and R. Osellame, Polarization Entangled State Measurement on a Chip, *Phys. Rev. Lett.* **105**, 200503 (2010).
- [35] X. Lu *et al.*, Chip-integrated visible-telecom entangled photon pair source for quantum communication, *Nat. Phys.* **15**, 373 (2019).
- [36] H. Jin *et al.*, On-Chip Generation and Manipulation of Entangled Photons Based on Reconfigurable Lithium-Niobate Waveguide Circuits, *Phys. Rev. Lett.* **113**, 103601 (2014).
- [37] H. Tang *et al.*, Experimental two-dimensional quantum walk on a photonic chip, *Sci. Adv.* **4**, eaat3174 (2018).
- [38] A. M. Goebel, C. Wagenknecht, Q. Zhang, Y.-A. Chen, K. Chen, J. Schmiedmayer, and J.-W. Pan, Multistage Entanglement Swapping, *Phys. Rev. Lett.* **101**, 080403 (2008).
- [39] J. Calsamiglia and N. Lütkenhaus, Maximum efficiency of a linear-optical Bell-state analyzer, *Appl. Phys. B* **72**, 67 (2001).
- [40] Y.-H. Kim, S. P. Kulik, and Y. Shih, Quantum Teleportation of a Polarization State with a Complete Bell State Measurement, *Phys. Rev. Lett.* **86**, 1370 (2001).
- [41] G. Kwiat and H. Weinfurter, Embedded Bell-state analysis, *Phys. Rev. A* **58**, R2623(R) (1998).
- [42] W. P. Grice, Arbitrarily complete Bell-state measurement using only linear optical elements, *Phys. Rev. A* **84**, 042331 (2011).
- [43] Y.-H. Kim, Quantum interference with beamlike type-II spontaneous parametric down-conversion, *Phys. Rev. A* **68**, 013804 (2003).
- [44] D. A. Willis, and V. Grosu, Microdroplet deposition by laser-induced forward transfer, *Appl. Phys. Lett.* **86**, 244103 (2005).
- [45] Y. Chen, J. Gao, Z.-Q. Jiao, K. Sun, W.-G. Shen, L.-F. Qiao, H. Tang, X.-F. Lin, and X.-M. Jin, Mapping Twisted Light into and Out of a Photonic Chip, *Phys. Rev. Lett.* **121**, 233602 (2018).
- [46] Y. Wang *et al.*, Topological protection of two-photon quantum correlation on a photonic chip, *Optica* **6**, 955 (2019).
- [47] J. Gao *et al.*, Experimental Collision-Free Dominant Boson Sampling, [arXiv:1910.11320](https://arxiv.org/abs/1910.11320).
- [48] X.-Y. Xu *et al.*, A scalable photonic computer solving the subset sum problem, *Sci. Adv.* **6**, eaay5853 (2020).
- [49] D. Rajan, and M. Visser, Quantum Blockchain Using Entanglement in Time, *Quantum Reports* **1**, 3 (2019).
- [50] Y. Cao, Y.-H. Li, K.-X. Yang, Y.-F. Jiang, S.-L. Li, X.-L. Hu, M. Abulizi, C.-L. Li, W. Zhang, Q.-C. Sun *et al.*, Long-Distance Free-Space Measurement-Device-Independent Quantum Key Distribution, *Phys. Rev. Lett.* **125**, 260503 (2020).
- [51] Y. Liu, Z. W. Yu, W. Zhang, J. Y. Guan, J. P. Chen, C. Zhang, X. L. Hu, H. Li, C. Jiang, J. Lin *et al.*, Experimental Twin-Field Quantum Key Distribution through Sending or Not Sending, *Phys. Rev. Lett.* **123**, 100505 (2019).
- [52] R.-J. Ren *et al.*, 128 Identical Quantum Sources Integrated on a Single Silica Chip, [arXiv:2005.12918](https://arxiv.org/abs/2005.12918).